Dyke Award. Imaging of Spinal CSF Pulsation by 2DFT MR: Significance During Clinical Imaging

Jeremy B. Rubin and Dieter R. Enzmann

AJNR Am J Neuroradiol 1987, 8 (2) 297-306
http://www.ajnr.org/content/8/2/297

Dyke Award

Imaging of Spinal CSF Pulsation by 2DFT MR: Significance During Clinical Imaging

Jeremy B. Rubin[1]
Dieter R. Enzmann

Understanding the MR appearance of spinal CSF is important in interpreting clinical spine images because the diagnosis of spinal pathology requires an accurate delineation of spinal CSF from spinal cord and thecal sac. During conventional 2DFT MR imaging of the spine, CSF pulsation caused two interdependent flow phenomena, signal loss and phase-shift images. Signal loss was observed as decreased signal intensity arising from pulsatile spinal CSF. Phase-shift images were observed as signal intensity arising from and morphologically identical to the spinal subarachnoid space but symmetrically displaced from it along the phase-encoding axis of MR images, either added to or subtracted from stationary signal intensity. These phenomena were common, occurring in most cervical and thoracic long-TR images. Both phenomena were less apparent in the lumbar region in most cases. CSF pulsation flow phenomena decreased CSF–spinal cord and CSF–thecal sac conspicuity, thereby obscuring normal and pathologic anatomy and, at times, simulating pathology. The areas of signal loss showed variable but characteristic patterns in the cervical and thoracic spine corresponding to regions of greatest flow. Signal loss in the axial plane was more pronounced when thin slices were used. Phase-shift images degraded overall image quality secondary to spatial mismapping of spinal CSF signal intensity. With the use of CSF gating, both signal loss and phase-shift images were eliminated. Understanding these features will be important in the accurate interpretation of MR spine images because analysis of CSF pulsation flow phenomena provides physiologic and pathologic information, and awareness of their existence avoids diagnostic confusion.

The appearance of spinal CSF in MR imaging has received little attention in the literature. With relatively thick slices (7–10 mm), reported signal intensity depended on the T1- or T2-weighting of the pulse sequence [1–10]. No reports on spinal CSF pulsation flow phenomena in MR are available in the literature, even though it is widely recognized that CSF pulsatile flow exists [11–19], and MR is extremely sensitive to flow [20–34].

Understanding the MR appearance of spinal CSF is crucial in interpreting clinical spine images because the diagnosis of spinal pathology requires an accurate delineation of spinal CSF from spinal cord and thecal sac. The ability to differentiate spinal CSF from adjacent structures explains the great utility of metrizamide CT in the evaluation of spinal diseases, although this procedure is not without risks [35, 36]. Complex CSF pulsation flow phenomena that occur during clinical MR spine imaging may alter spinal CSF signal intensity, either obscuring normal or pathologic anatomy, or occasionally simulating pathology (Fig. 1).

In part 1 of this article, we describe the appearance and frequency of spinal CSF pulsation phenomena on MR of normal and pathologic spines. In part 2 [37], a new spine phantom is used for quantitative analysis of these phenomena. This combination of studies permits an in-depth understanding of the complex signal patterns observed clinically during MR.

This article appears in the March/April 1987 issue of *AJNR* and the May 1987 issue of *AJR*.

Received March 31, 1986; accepted after revision September 16, 1986.

Presented at the annual meeting of the American Society of Neuroradiology, San Diego, January 1986, and the Western Neuroradiological Society, Monterey, CA, October 1985.

[1] Both authors: Department of Radiology, Stanford University School of Medicine, Stanford, CA 94305. Address reprint requests to J. B. Rubin.

***AJNR* 8:297–306, March/April 1987**
0195–6108/87/0802–0297

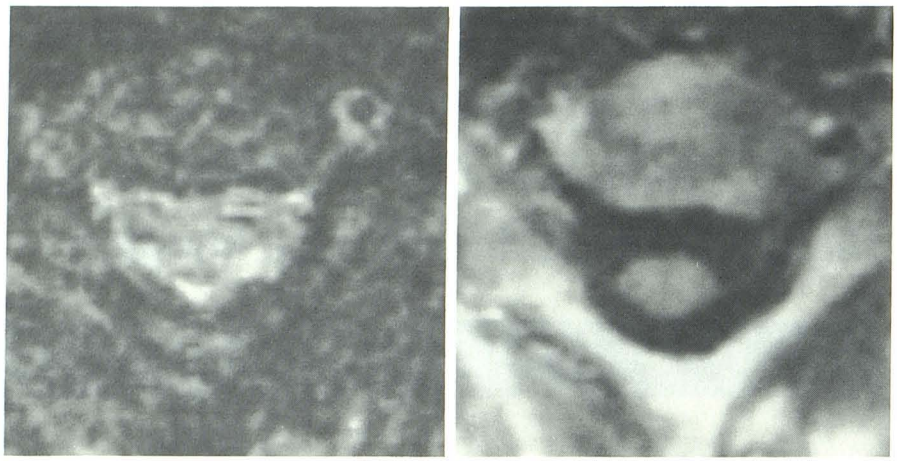

Fig. 1.—Normal cervical spine. Confusing images created by CSF pulsatile flow.

***A*, Axial long-TR pulse sequence with complex spinal CSF signal intensity. TR 2500 msec, TE 80 msec, slice thickness 3 mm. High-, medium-, and low-intensity spinal CSF surrounded spinal cord and obscured its margins. This image shows difficulty frequently encountered in interpretation of thin-section long-TR spinal images.**

***B*, Axial short-TR pulse sequence at same level. TR 400 msec, TE 25 msec, slice thickness 10 mm. Low signal intensity of spinal CSF delineated spinal cord margins.**

Subjects and Methods

A GE Signa superconducting MR imaging system operating at 1.5 T was used in conjunction with a 30- by 18-cm rectangular or 20-cm circular surface coil for all spine studies. 2DFT spin-echo multislice imaging was used with short and long repetition times (TRs). Short-TR sequences (400–600 msec) used an echo time (TE) of 25 msec with two or four excitations. Long-TR (2000–3000 msec) sequences used either symmetric echoes (TE 40 and 80 msec) or asymmetric echoes (TE 25 and 80 msec) with two excitations. Image matrix size was 256 in both the frequency and phase-encoding directions. Slice thickness was 3 or 5 mm during routine imaging and 10 or 20 mm during selected studies. Slice spacing was 20% of slice thickness. Field of view ranged from 16 to 32 cm depending on imaging plane.

We evaluated 154 patients aged 4–81 years who were referred for suspected disease of the cervical, thoracic, or lumbar spine. In each case, a sagittal short-TR sequence was obtained; subsequent pulse sequences depended on patient history and demonstration of pathology, but generally included axial short-TR and axial and/or sagittal long-TR sequences. In four normal patients, axial long-TR sequences were obtained with slice thicknesses of 3, 5, 10, and 20 mm. In three normal volunteers gated axial and sagittal images of the cervical or thoracic spine were compared with nongated pulse sequences. Gating was performed with an infrared detector fixed to the fingertip that recorded systolic capillary blushing (Medasonics Model PPG-13, Mountain View, CA). Gated data acquisition was triggered after a delay of about 500 msec from the detection of the physiologic pulse.

Patients were segregated into three groups (normal thecal sac, mild to moderately narrowed thecal sac, and severely narrowed thecal sac) on the basis of MR images, clinical history, correlative studies (including CT and myelography), and surgical results if available. Criteria for inclusion in the normal group were a normal-appearing thecal sac and spinal cord. Patients were allocated to the mild to moderately narrowed thecal sac group when degenerative disease or neoplasm narrowed but did not obliterate the subarachnoid space. Allocation to the severely narrowed thecal sac group required significant narrowing of the subarachnoid space. The appearance of the spinal CSF signal intensity was not used as a criterion for classification. Patients in the mild-moderately and severely narrowed thecal sac groups had any of several diagnoses: herniated nucleus pulposus, spinal stenosis, astrocytoma, syrinx, meningioma, and tuberculous osteomyelitis. Each group was analyzed separately for CSF signal intensity and homogeneity within the subarachnoid space, and for the presence of phase-shift images anterior and posterior to the spinal canal.

Results

Two CSF pulsation flow phenomena were observed on clinical images: signal loss and phase-shift images (Figs. 2 and 3). Signal loss was observed as decreased signal intensity arising from pulsatile spinal CSF. Phase-shift images were observed as signal intensity arising from and morphologically identical to the spinal subarachnoid space but symmetrically displaced from it along the phase-encoding axis of MR images, either added to or subtracted from stationary signal intensity. The manifestations of these pulsation flow phenomena on a given image depended on numerous factors including spinal segment, imaging plane, TR, TE, slice thickness, echo number, and spinal pathology (Table 1). In general, these phenomena were most common in the cervical and thoracic spinal segments when long-TR pulse sequences were used. They were observed less often in the lumbar spine (Fig. 4). Signal loss and phase-shift images were observed on short-TR sequences in only eight of 107 normal spines, although their conspicuity depended in part on the image window and level settings selected for photography.

Signal loss was observed in the axial plane of normal cervical and thoracic spines on long-TR pulse sequences in all patients (Table 1). In no patient was signal loss observed on axial long-TR images in the lumbar region. The pattern of CSF signal loss in relation to the spinal cord depended on the position of the spinal cord in relation to the subarachnoid space (Figs. 2C, 2D, and 5), and this in turn depended on the spinal level imaged. In the cervical spine, signal loss appeared as regions of decreased spinal CSF signal intensity either anterior and anterolateral to the spinal cord (Figs. 2C, 2G, and 2H) or circumferentially around the spinal cord (Fig. 2E). In the thoracic spine, signal loss appeared as regions of decreased signal intensity either posterior and posterolateral to the spinal cord or circumferentially around the spinal cord.

TABLE 1: Spinal Subarachnoid Space: Observed CSF Signal Loss and Phase-Shift Images

Group: Spinal Segment	Axial Images		Sagittal Images	
	First Echo	Second Echo	First Echo	Second Echo
Normal (n = 107):				
Cervical (n = 41):				
% Signal loss	100	100	90	85
% Phase-shift images	34	34	100	100
Thoracic (n = 27):				
% Signal loss	100	100	100	89
% Phase-shift images	19	19	100	100
Lumbar (n = 39):				
% Signal loss	0	0	0	0
% Phase-shift images	0	0	15	15
Mild to moderate narrowing (n = 33):				
Cervical (n = 13):				
% Signal loss	100	100	92	92
% Phase-shift images	23	23	100	100
Thoracic (n = 5):				
% Signal loss	100	100	100	100
% Phase-shift images	0	0	100	100
Lumbar (n = 15):				
% Signal loss	0	0	0	0
% Phase-shift images	0	0	0	0
Severe narrowing (n = 14):				
Cervical (n = 5):				
% Signal loss	0	0	0	0
% Phase-shift images	0	0	0	20
Thoracic (n = 3):				
% Signal loss	0	0	0	0
% Phase-shift images	0	0	33	33
Lumbar (n = 6):				
% Signal loss	0	0	0	0
% Phase-shift images	0	0	0	0

Signal loss on axial cervical and thoracic spinal images was slightly more prominent on second-echo than on first-echo images. The presence of signal loss in the axial plane impaired delineation of CSF interfaces with both spinal cord and thecal sac (Figs. 2C and 2E).

Signal loss was observed in the sagittal plane of normal cervical and thoracic spines on long-TR pulse sequences in 85–100% of patients depending on spinal segment and echo number (Table 1). In no patient was signal loss observed on sagittal long-TR images in the lumbar spine. The pattern of CSF signal loss in relation to the spinal cord closely reflected the appearance described on axial images. In the cervical spine, signal loss appeared as curvilinear bands of decreased signal intensity, predominantly anterior to the spinal cord or within the lateral recesses, depending on the relationship of the imaging plane to midline (Figs. 2A, 2B, and 2F). In the thoracic spine, signal loss was observed as curvilinear bands of decreased signal intensity predominantly posterior or lateral to the spinal cord, also depending on the relationship of the imaging plane to midline (Fig. 3). Signal loss on sagittal images was less prominent on second-echo than on first-echo images using symmetric-echo pulse sequences. In contrast, signal loss was more prominent on second-echo images when asymmetric pulse sequences were used. The presence of signal loss in the sagittal plane impaired delineation of CSF interfaces with both spinal cord and thecal sac (Figs. 2A, 2B, and 3).

Phase-shift images were observed in the sagittal plane of normal cervical and thoracic spines on long-TR pulse sequences in all patients (Table 1). In only 15% of normal patients were phase-shift images observed in the lumbar region on sagittal long-TR images. In the sagittal plane, phase-shift images appeared as curvilinear bands of either increased or decreased signal intensity morphologically identical to the spinal subarachnoid space but projected symmetrically from it both anteriorly and posteriorly along the phase-encoding direction (Fig. 2B). When projected into air anterior or posterior to the cervical spine, phase-shift images consisted of uniformly increased signal intensity. On midline images, phase-shift images arose from CSF both anterior and posterior to the spinal cord. When superimposed on the spinal cord or other structures anterior or posterior to the spinal canal, phase-shift images resulted in a "striated" pattern, degrading overall image quality and impairing delineation of CSF interfaces with both spinal cord and thecal sac (Figs. 2B and 2F). Phase-shift images in the sagittal plane were less prominent on second-echo than on first-echo images using symmetric-echo pulse sequences. In contrast, phase-shift images were more prominent on second-echo images when asymmetric-echo pulse sequences were used.

Phase-shift images were observed in the axial plane of normal spines on long-TR pulse sequences in 34% of cervical and 19% of thoracic spines (Table 1). In no patients were phase-shift images observed in the lumbar spine on axial

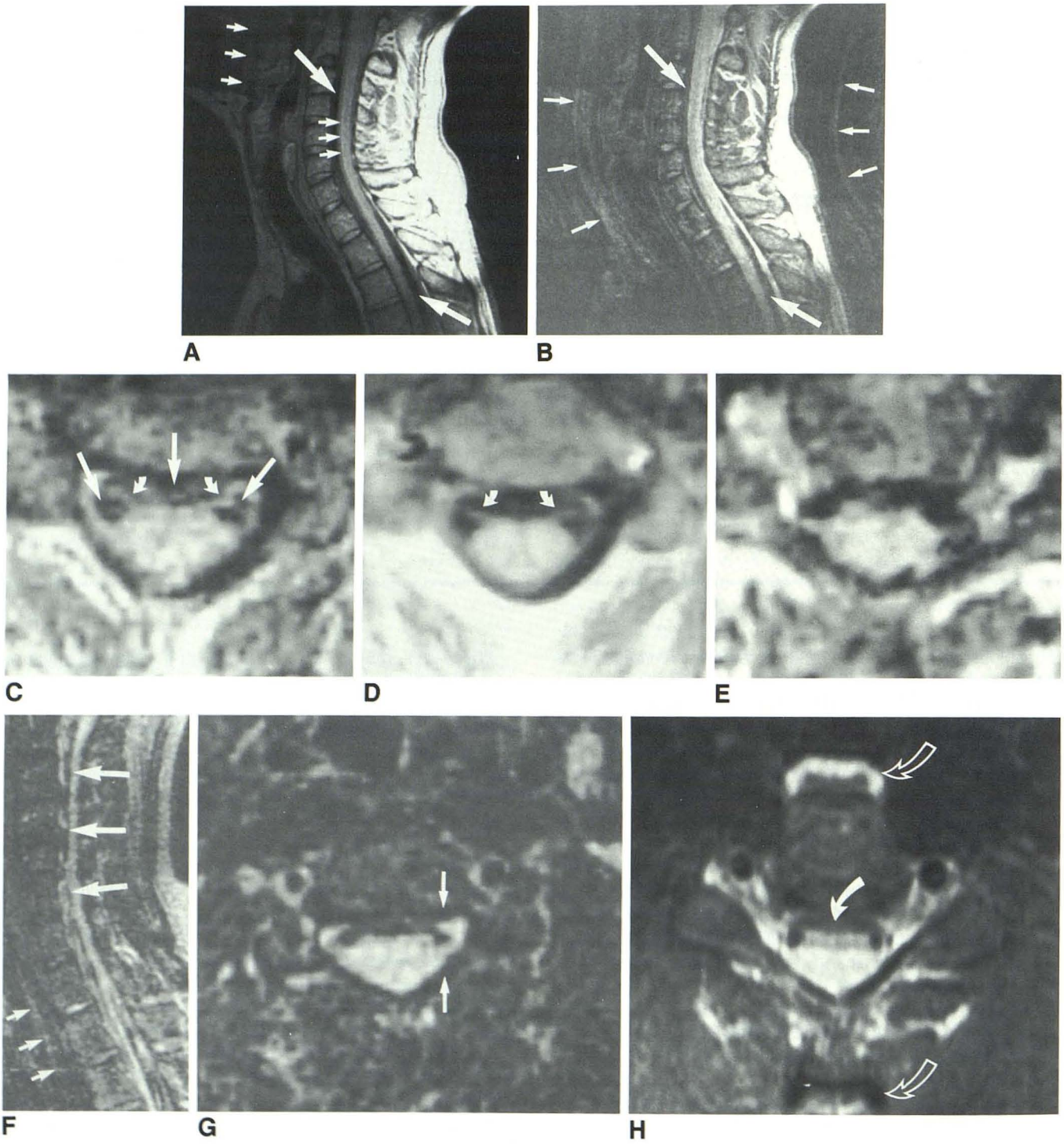

Figure 2. See caption, opposite page.

◀ **Fig. 2.—Normal cervical spine. Manifestations of CSF pulsatile flow.**

***A*, Sagittal long-TR first-echo image shows signal loss and phase-shift images. TR 2500 msec, TE 25 msec, slice thickness 3 mm. With these imaging parameters, CSF signal intensity should be equal to or greater than spinal cord signal intensity. Signal loss (*long arrows*) of CSF was present anterior to upper cervical cord and posterior to lower cervical cord. Phase-shift images were projected onto spinal cord (*short arrows*) and anterior to spine (*short arrows*).**

***B*, Sagittal long-TR second-echo image shows more pronounced signal loss and phase-shift images using asymmetric echoes. TR 2500 msec, TE 80 msec, slice thickness 3 mm. Signal loss (*long arrows*) and phase-shift images (*short arrows*) were increased relative to first-echo image (*A*). Superimposition of phase-shift images on spinal cord degraded its visualization.**

***C*, Axial long-TR first-echo image shows signal loss. TR 2000 msec, TE 40 msec, slice thickness 3 mm. Signal loss (*straight arrows*) was localized to anterolateral recesses and anterior subarachnoid space because of posterior spinal cord position. Anterior nerve roots (*curved arrows*) were seen within anterolateral recesses.**

***D*, Comparison axial short-TR pulse sequence at same level shows normal anatomy. TR 600 msec, TE 25 msec, slice thickness 3 mm. Regions of signal loss on long-TR image (*C*) were shown to correspond to spinal CSF. Anterior nerve roots (*arrows*) were better seen and appeared smaller.**

***E*, Axial long-TR first-echo image shows irregular spinal cord contour. TR 2500 msec, TE 40 msec, slice thickness 3 mm. Circumferential signal loss was most pronounced anteriorly and within anterolateral recesses because CSF motion was greatest in these regions. More slowly moving CSF adjacent to spinal cord was isointense with cord and obscured actual cord margin.**

***F*, Sagittal long-TR second-echo image shows signal loss and phase-shift images. TR 2000 msec, TE 80 msec, slice thickness 3 mm. Imaging plane was through left anterolateral recess, lateral to spinal cord. Signal loss (*long arrows*) appeared as curvilinear band of decreased signal intensity adjacent to more slowly moving CSF within anterolateral recess. Phase-shift images (*short arrows*) were seen anteriorly.**

***G*, Comparison axial long-TR second-echo image. TR 2500 msec, TE 80 msec, slice thickness 3 mm. Characteristic signal loss anteriorly and within anterolateral recesses bilaterally. *Arrows* indicate sagittal imaging plane of *F*.**

***H*, Axial long-TR second-echo image shows signal loss and phase-shift images. TR 1200 msec, TE 40 msec, slice thickness 5 mm. Characteristic signal loss (*solid arrow*) anterior and anterolateral to spinal cord. Phase-shift images (*open arrows*) were symmetrically displaced from subarachnoid space anteriorly and posteriorly. Both were morphologically identical to signal loss within subarachnoid space. Anterior phase-shift image was added to soft-tissue signal intensity, whereas posterior phase-shift image was subtracted from soft-tissue signal intensity. Numerous, less intense phase-shift images were also present.**

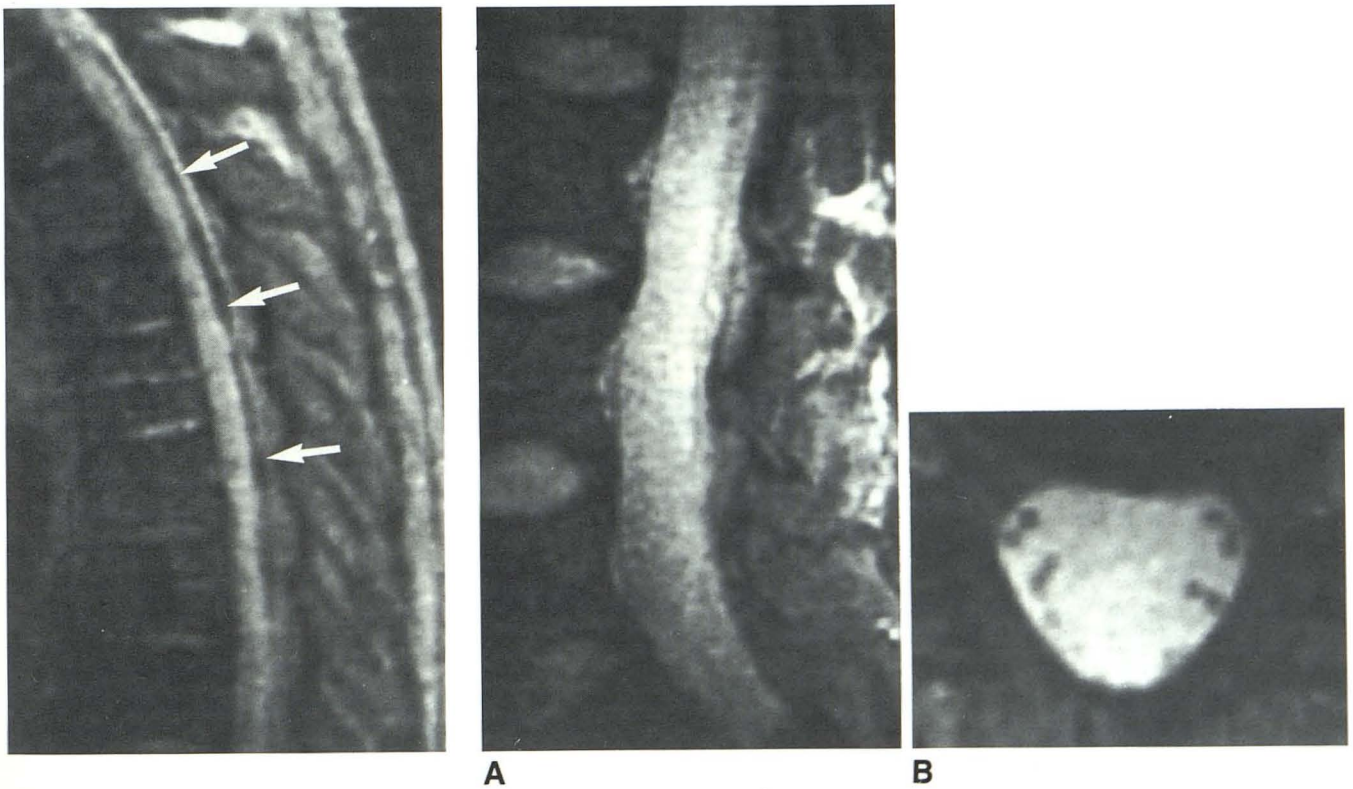

Fig. 3.—Normal thoracic spine. Manifestations of CSF pulsation flow phenomena. Sagittal long-TR second-echo image shows signal loss. TR 2000 msec, TE 80 msec, slice thickness 3 mm. Broad curvilinear band of signal loss (*arrows*) was predominantly posterior to spinal cord because of anterior cord position. Signal loss anterior to the cord is difficult to separate from cortical bone of posterior vertebral body, which also is low signal intensity.

Fig. 4.—Normal lumbar spine. Absent CSF pulsation flow phenomena.

***A*, Sagittal long-TR second-echo image shows high signal intensity of CSF within thecal sac. TR 2500 msec, TE 80 msec, slice thickness 3 mm. Nonuniformity of signal was secondary to surface-coil imaging. No signal loss or phase-shift images were present.**

***B*, Corresponding axial long-TR second-echo image shows high signal intensity of CSF within thecal sac. TR 2500 msec, TE 80 msec, slice thickness 3 mm. Paired nerve roots were well delineated in absence of signal loss and phase-shift images.**

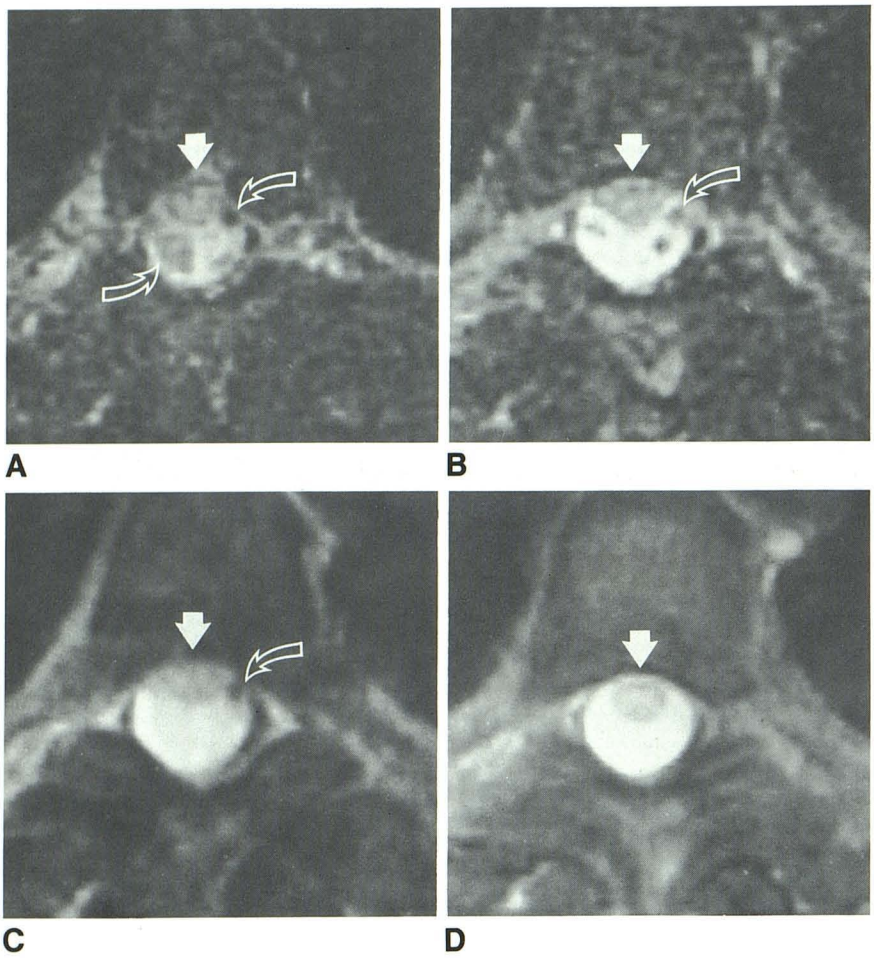

Fig. 5.—Normal thoracic spine. Signal loss simulating intradural masses; effect of slice thickness on signal loss.

***A*, Axial long-TR second-echo image shows variegated regions of signal loss within thecal sac. TR 2000 msec, TE 80 msec, slice thickness 3 mm. Spinal cord (*solid arrow*) was difficult to differentiate from regions of signal loss (*open arrows*), which varied in intensity.**

***B*, Axial long-TR second-echo image at different level shows variation in size, position, and signal intensity of circumscribed regions of signal loss. TR 2000 msec, TE 80 msec, slice thickness 3 mm. Large circumscribed region of signal loss in *A* was absent at this level. Smaller region of signal loss laterally persisted (*open arrow*). Spinal cord (*solid arrow*) was unchanged in appearance.**

***C*, Axial long-TR second-echo image at same level as *B* shows effect of increasing slice thickness on signal loss. TR 2000 msec, TE 80 msec, slice thickness 10 mm. All regions of signal loss disappeared except one (*open arrow*). Spinal cord contour (*solid arrow*) was better delineated.**

***D*, Axial long-TR second-echo image at same level as *C* shows effect of further increasing slice thickness. TR 2000 msec, TE 80 msec, slice thickness 20 mm. All regions of signal loss are now eliminated; CSF signal intensity is uniform. Spinal cord contour and size are well delineated (*arrow*).**

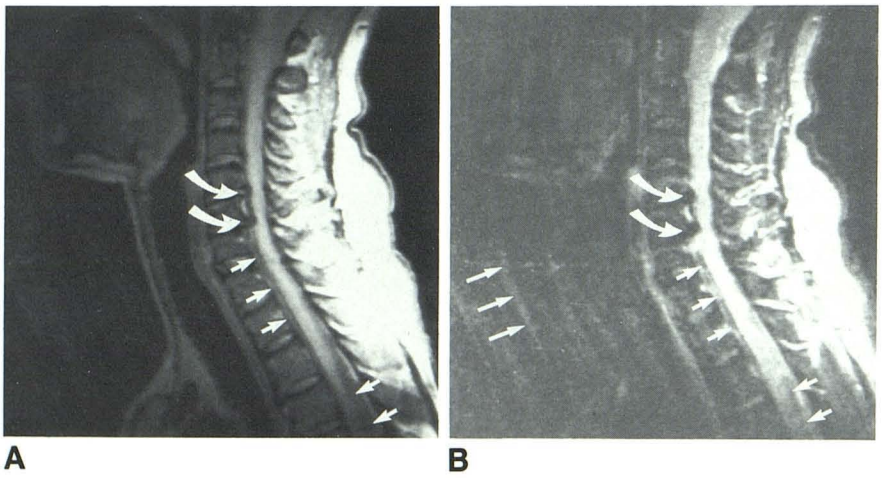

Fig. 6.—Anterior cervical osteophytes. Effect of incomplete spinal block on signal loss and phase-shift images.

***A*, Sagittal long-TR first-echo image shows signal loss caudal to cervical osteophytes. TR 2500 msec, TE 25 msec, slice thickness 3 mm. Cervical osteophytes (*curved arrows*) at C5–C6 and C6–C7. Signal loss (*straight arrows*) caudal to osteophytes indicates lesions were not causing high-grade block.**

***B*, Corresponding long-TR second-echo sagittal image shows signal loss and phase-shift images below cervical osteophytes. TR 2500 msec, TE 80 msec, slice thickness 3 mm. In addition to signal loss (*short straight arrows*), phase-shift images (*long straight arrows*) were present caudal to osteophytes (*curved arrows*). This figure illustrates the utility of demonstrating pulsation flow phenomena in evaluating degree of spinal block.**

long-TR images. In the axial plane, phase-shift images appeared as "crescents" or "rings" of increased or decreased signal intensity morphologically identical to the spinal subarachnoid space but projected symmetrically from it both anteriorly and posteriorly along the phase-encoding direction (Fig. 2H). When projected into air anterior or posterior to the cervical spine, phase-shift images consisted of uniformly increased signal intensity.

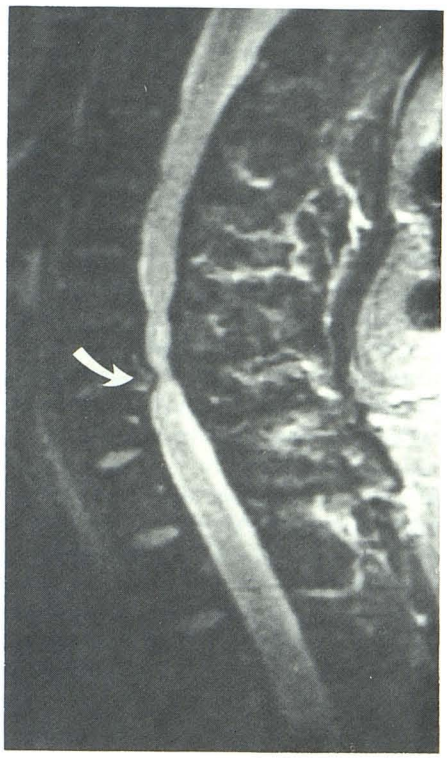

Fig. 7.—Herniated nucleus pulposus. Effect of high-grade block on signal loss and phase-shift images. Sagittal long-TR second-echo image shows absence of pulsation flow phenomena in patient with herniated disk at C6–C7 (*arrow*), which caused high-grade spinal block. TR 2500 msec, TE 80 msec, slice thickness 3 mm. Note absence of signal loss and phase-shift images caudal to lesion. In absence of these pulsation flow phenomena, CSF–thecal sac and CSF–spinal cord conspicuity were excellent. Pulsation flow phenomena were absent because CSF pulsation amplitude was decreased by spinal block. This figure illustrates utility of demonstrating absence of pulsation flow phenomena in cases of high-grade spinal block. Care must be taken to ensure that accidental pseudogating does not occur.

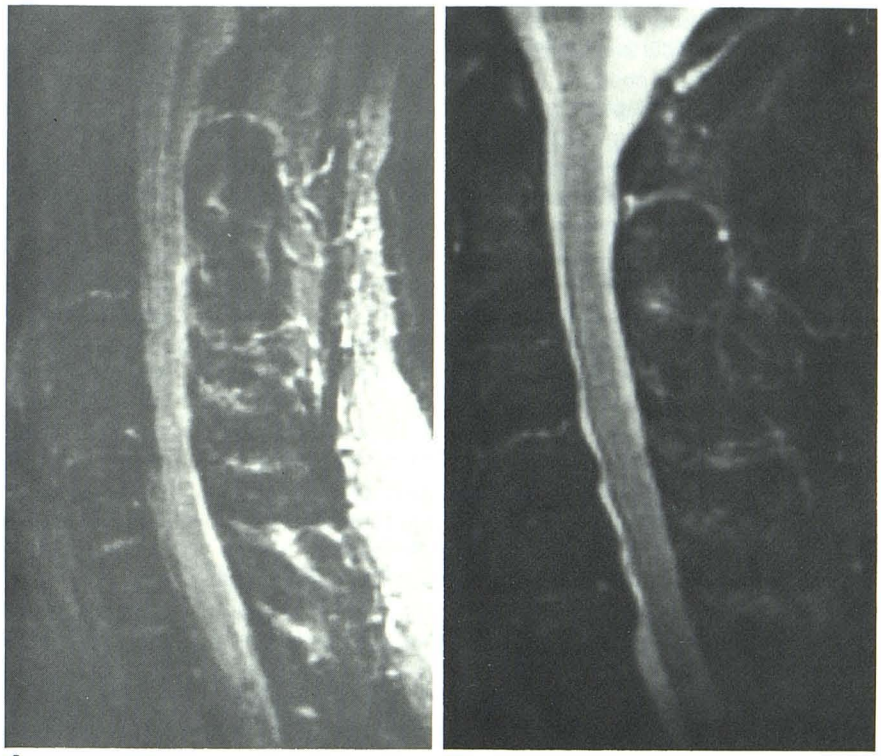

A B

Fig. 8.—Cervical spondylosis. Effect of CSF gating on pulsatile flow phenomena.

A, Long-TR second-echo sagittal image (nongated) shows characteristic signal loss and phase-shift images. TR 2500 msec, TE 80 msec, slice thickness 3 mm. Pulsatile flow phenomena result in decreased conspicuity of thecal sac and spinal cord as well as generalized decrease in image quality.

B, Single-slice sagittal CSF-gated image eliminated pulsatile flow phenomena. Effective TR about 850 msec, TE 80 msec, slice thickness 5 mm. Signal loss and phase-shift images were absent. "Myelographic" effect permitted accurate delineation of thecal sac and spinal cord revealing cervical spondylitic changes poorly seen on nongated image (*A*). Acquisition time for this image was about one-third that required for nongated study.

In 33 patients classified with mild to moderate narrowing of the spinal subarachnoid space (Fig. 6), signal loss and phase-shift images were observed with comparable frequency and identical pattern to the normal group when imaged below the level of narrowing (Table 1). In several cases, signal loss at the level of narrowing was slightly more prominent than above or below the narrowed segment. When narrowing of the subarachnoid space was severe, signal loss and phase-shift images were absent below the level of narrowing (Fig. 7) in most of the patients.

Increasing slice thickness from 3 to 20 mm during axial imaging of normal cervical and thoracic spines in four normal patients resulted in decreased signal loss and increased uniformity of subarachnoid CSF signal intensity. With a 20-mm thickness, signal loss was completely eliminated (Fig. 5). Cardiac gating in three volunteers eliminated signal loss and phase-shift images while reducing imaging time (Fig. 8). Elimination of the CSF pulsation flow phenomenon resulted in improved delineation of spinal cord and thecal sac margins and overall improvement in image quality.

Discussion

The existence of spinal CSF pulsation has been widely recognized and extensively evaluated by both manometric [16–19] and myelographic [11–15] methods. It is also well known that the MR signal is extremely sensitive to motion [20–34]. It is therefore not unexpected that spinal CSF pulsation causes changes on MR, although a description of spinal CSF pulsatile flow phenomena has not yet been reported. Until these CSF pulsation phenomena are understood, they can hinder diagnoses by obscuring normal or pathologic anatomy or occasionally simulating pathology. MR of the

spine provides new insights into CSF flow in the spinal canal that are apparent particularly when long-TR pulse sequences are used.

CSF pulsation flow phenomena obscure CSF–spinal cord and CSF–thecal sac interfaces and reduce overall image quality. In the cervical spine, osteophytes, degenerative disks, and CSF pulsation signal loss are all low in signal intensity, making differentiation difficult. In the thoracic spine, CSF pulsation signal loss can assume different shapes secondary to differing flow rates around nerve roots and arachnoid septations that can result in the simulation of masses. It is conceivable that a spinal AVM could be simulated by normal CSF pulsation signal loss or be overlooked if enlarged vascular structures were located close to regions of CSF pulsation signal loss. It is also possible for CSF pulsation phase-shift images to obscure subtle spinal cord lesions on long-TR sequences when superimposed on the spinal cord. Some of these pitfalls are avoidable once CSF pulsation signal loss and phase-shift images are understood. In addition, understanding the etiology of these CSF pulsation flow phenomena provides a rational approach to eliminating them. Both phenomena occur secondary to harmonic modulation of proton precessional phase by the oscillatory CSF motion, as is described in detail in part 2 of this article [37].

Spinal CSF pulsation is characterized by an oscillatory motion of subarachnoid spinal CSF that is synchronous with the cardiac cycle [11–19]. When observed myelographically, an inferior displacement of oily contrast coincides with the onset of systole and ceases with diastole [11, 12]. It is believed that this motion results from systolic expansion of the brain, which displaces CSF from the cranial vault into the spinal subarachnoid space. Quantitatively, it is estimated that 2.5 ml of CSF is displaced from the cranial vault with each heartbeat [12]. The excess fluid is accommodated within the spinal canal by the lumbar epidural venous plexus, which provides the necessary compliance in an otherwise rigid system. Venous influences on CSF pulsation are also widely recognized, although these are most important during disease states (hydrocephalus and congestive heart failure) or physiologic maneuvers (Valsalva, hyperventilation, and cough) [11, 12, 16].

Myelographic studies have revealed that CSF pulsation amplitude is greatest in the cervical region (3–30 mm, mean 9.6 mm), smaller in the thoracic region, and least in the lumbar region (0–7 mm, mean 1.7 mm) [11–13]. This agrees completely with our observations as reflected in the frequency of signal loss and phase-shift images in the normal patient group. Myelographic studies have also shown increased pulsation amplitude at the level of incomplete spinal blocks, diminished pulsation amplitude proximal to complete spinal blocks, and absent pulsation distal to complete spinal blocks [11–13]. These findings have also been confirmed on MR images from our abnormal patient groups. The severity of subarachnoid space narrowing on MR images may be exaggerated because locally increased CSF velocity within the narrowed subarachnoid space enhances signal loss. Exclusion of complete block depends on demonstration of pulsation flow phenomena distal to the lesion. In cases of high-grade or complete spinal block, homogeneous increased CSF signal intensity is observed distal to the block without signal loss or phase-shift images. When CSF pulsation flow phenomena are absent, however, it is necessary to differentiate stationary CSF from chance pseudogating and incomplete even-echo rephasing. Pseudogating represents a chance synchronization between the CSF pulsation period and TR that minimizes CSF pulsation flow phenomena. Incomplete even-echo rephasing produces higher CSF signal intensity on sagittal second-echo images than on first-echo images simulating relatively stationary CSF, and is discussed further in part 2 of this article [37]. Understanding these CSF dynamics and flow phenomena will be important in the accurate interpretation of MR spinal images because they provide physiologic and pathologic information similar to that obtained by more invasive means such as myelography.

The pattern of CSF pulsation signal loss observed at a given level depends on the interaction between CSF flow and subarachnoid anatomy (spinal cord position within the thecal sac, nerve roots, and arachnoid septations). As will be shown in part 2 of this article, the magnitude of signal loss within pulsatile CSF is quantitatively related to flow velocity (during both axial and sagittal imaging) in addition to slice thickness (during axial imaging). Anatomic factors influencing the pattern of subarachnoid signal loss are somewhat less predictable. Spinal cord position is variable but often determined by the normal cervical lordosis (posterior cord) and thoracic kyphosis (anterior cord). CSF flow around the spinal cord is complex probably because nerve roots and arachnoid septations function as "hydraulic baffles" that locally slow CSF flow, create turbulence, and channel CSF into unobstructed regions of the subarachnoid space. Variability of CSF pulsation signal loss between patients is likely related in part to differences in CSF flow velocity and the development of their arachnoid septations [38]. In extreme cases, CSF may be relatively stagnant within arachnoid septations, most often within the dorsal thoracic spine [38]. In some regions of the subarachnoid space there appears to be less variability in the appearance of CSF pulsation signal loss, probably because in these regions CSF flow is relatively unobstructed ("CSF flow channels"). Prominent CSF pulsation signal loss in the cervical anterolateral recesses is a relatively constant finding in most patients, suggesting these regions may function as CSF flow channels.

Recognition of signal loss within CSF flow channels in the cervical and thoracic spine is facilitated by the presence of higher signal intensity within adjacent stagnant CSF. Slower-flowing CSF occurs at the CSF–thecal sac and CSF–spinal cord interfaces because of hydrodynamic considerations [39, 40], leading to less pronounced signal loss. Unfortunately, this signal intensity is often isointense with adjacent structures making delineation of the true interface difficult if not impossible with long-TR sequences. The lower pulsation amplitude of CSF within the lumbar spine accounts in part for the decreased incidence of signal loss at this level. Recognition of signal loss within the lumbar spine may be more difficult than it is within other spinal segments, however. Some signal loss within the lumbar CSF may be present but unrecognized,

because absence of CSF flow channels in the lumbar spine precludes comparison of moving CSF with relatively stagnant CSF. In fact, cases of arachnoid cysts in the lumbar region demonstrate higher signal intensity of CSF within the cyst, suggesting that signal loss within the lumbar spine is likely to be underestimated in our series.

Phase-shift-image appearance (intensity, discreteness, number, and position) and signal loss are highly variable between patients. As is demonstrated in part 2 of this article [37], phase-shift-image number and position is influenced by the relationship between heart rate and TR, whereas its intensity is influenced by CSF pulsation amplitude. Differences between patients are therefore dependent on both physiologic (heart rate, arrhythmias, CSF pulsation amplitude, subarachnoid anatomy) and imaging (TR) parameters. It is important to recognize that much of the variability observed in the appearance of CSF pulsation flow phenomena occurs secondary to chance synchronization of data acquisition (TR) with the cardiac cycle, which explains why these phenomena are occasionally not observed. In addition, symmetric- and asymmetric-echo pulse sequences result in different appearances of CSF on sagittal second-echo images [41], as was observed in this patient group. Phase-shift images originating from pulsatile CSF motion should be differentiated from other kinds of phase-shift signal, which arise from any form of periodic motion (swallowing, cardiac, respiratory, blood flow, and bowel). The most reliable distinguishing feature between these and CSF phase-shift images is that the latter are morphologically identical to the corresponding signal loss within the subarachnoid space and are confined to planes containing pulsatile CSF.

In view of the numerous publications concerning MR of the spine [1–10], at first it is unclear why a phenomenon such as spinal CSF pulsation, which is so fundamental, has not yet been reported. This is likely related in part to TR and slice thickness during axial imaging. Review of recent literature revealed that long-TR sequences were not routinely obtained in most studies, and slice thicknesses of 7–15 mm were generally used. As we have demonstrated, these phenomena are most prominent on long-TR pulse sequences and in the axial plane, particularly when thin sections are imaged. They are less evident on short-TR pulse sequences in which CSF has little intrinsic signal because of its long T1. It is also possible that these phenomena were not observed as often on early imagers because heavily T2-weighted images were more difficult to obtain with an acceptable signal-to-noise ratio. Long TR pulse sequences are useful in spine imaging because T2 contrast can sometimes demonstrate cord lesions or low-intensity extradural defects that may not be apparent when imaged with short-TR sequences [42].

To improve demonstration of spinal CSF and quantitatively evaluate normal and abnormal CSF dynamics, MR CSF flow imaging may be useful with flow-sensitive pulse sequences. However, CSF flow imaging for the purpose of inferring anatomic detail may prove unpredictable in many patients because variations in normal subarachnoid anatomy may lead to nonuniform flow patterns. With the advent of CSF gating, anatomic detail is obtained irrespective of CSF flow and arachnoid septations. The elimination of both signal loss and phase-shift images results in improved CSF–spinal cord and CSF–thecal sac conspicuity in addition to overall improved image quality secondary to an increased signal-to-noise ratio. The clinical implementation of CSF gating is described elsewhere [41, 42]. The rationale for its application to MR spinal imaging follows directly from theoretical considerations described in detail in part 2 of this article [37].

ACKNOWLEDGMENT

We thank Alan Wright for assistance in implementing gating on the GE Signa system.

REFERENCES

1. Hyman RA, Edwards JH, Vacirca SJ, Stein HL. 0.6 T MR imaging of the cervical spine: multislice and multiecho techniques. *AJNR* **1985**;6:229–236
2. Norman D, Mills CM, Brant-Zawadzki M, Yeates A, Crooks LE, Kaufman L. Magnetic resonance imaging of the spinal cord and canal: potentials and limitations. *AJNR* **1984**;5:9–14
3. Modic MT, Weinstein MA, Pavlicek W, Boumphrey F, Starnes D, Duchesneau PM. Magnetic resonance imaging of the cervical spine: technical and clinical observations. *AJNR* **1984**;5:15–22
4. Modic MT, Weinstein MA, Pavlicek W, et al. Nuclear magnetic resonance imaging of the spine. *Radiology* **1983**;148:757–762
5. Han JS, Kaufman B, El Yousef SJ, et al. NMR imaging of the spine. *AJR* **1983**;141:1137–1145, *AJNR* **1983**;4:1151–1159
6. Maravilla KR, Lesh P, Weinreb JC, Selby DK, Mooney V. Magnetic resonance imaging of the lumbar spine with CT correlation. *AJNR* **1985**;6:237–245
7. Modic MT, Pavlicek W, Weinstein MA, et al. Magnetic resonance imaging of intervertebral disk disease. Clinical and pulse sequence considerations. *Radiology* **1984**;152:103–111
8. Chafetz NI, Genant HK, Moon KL, Helms CA, Morris JM. Recognition of lumbar disk herniation with NMR. *AJR* **1983**;141:1153–1156, *AJNR* **1984**;5:23–26
9. Lee BC, Zimmerman RD, Manning JJ, Deck MD. MR imaging of syringomyelia and hydromyelia. *AJNR* **1985**;6:221–228
10. Yeates A, Brant-Zawadzki M, Norman D, Kaufman L, Crooks LE, Newton NH. Nuclear magnetic resonance imaging of syringomyelia. *AJNR* **1983**;4:234–237
11. Du Boulay GH. Pulsatile movements in the CSF pathways. *Br J Radiol* **1966**;39:255–262
12. Du Boulay GH. Specialization broadens the view. The significance of a CSF pulse. *Clin Radiol* **1972**;23:401–409
13. Lane B, Kricheff II. Cerebrospinal fluid pulsations at myelography: a videodensitometric study. *Radiology* **1974**;110:579–587
14. Gilland O, Chin F, Anderson WB, Nelson JR. A cinemyelographic study of cerebrospinal fluid dynamics. *AJR* **1969**;106:369–375
15. Reitan H. On movements of fluid inside the cerebrospinal space. *Acta Radiol* (Stockh) **1941**;22:762–779
16. Dardenne G, Dereymaeker A, Lacheron JM. Cerebrospinal fluid pressure and pulsatility. An experimental study of circulatory and respiratory influences in normal and hydrocephalic dogs. *Eur Neurol* **1969**;2:192–216
17. Adolph RS, Fukusumi H, Fowler NO. Origin of cerebrospinal fluid pulsations. *Am J Physiol* **1967**;212:840–846
18. Gilland O, Tourtellotte WW, O'Tauma L, Henderson WG. Normal cerebrospinal fluid pressure. *J Neurosurg* **1974**;40:587–593
19. Ekstedt J. CSF hydrodynamic studies in man. *J Neurol Neurosurg Psychiatry* **1978**;41:345–353
20. Hahn EL. Detection of sea water motion by nuclear precession. *J Geophys Res* **1960**;65:776–777
21. Carr HY, Purcell EM. Effects of diffusion on free precession in nuclear magnetic resonance experiments. *Phys Rev* **1954**;94:630–638
22. Suryan G. Nuclear resonance in flowing liquids. *Proc Indian Acad Sci* **1951**;33:107–111

23. von Schulthess GK, Fisher M, Crooks LE, Higgins CB. Gated MR imaging of the heart: intracardiac signals in patients and healthy subjects. *Radiology* **1985**;156:125–132
24. Mills CM, Brant-Zawadzki M, Crooks LE, et al. Nuclear magnetic resonance: principles of blood flow imaging. *AJNR* **1983**;4:1161–1166
25. Crooks LE, Mills CM, Davis PL, et al. Visualization of cerebral and vascular abnormalities by NMR imaging. The effects of imaging parameters on contrast. *Radiology* **1982**;144:843–852
26. von Schulthess GK, Higgins CB. Blood flow imaging with MR: spin-phase phenomena. *Radiology* **1985**;157:687–695
27. Bradley WG, Waluch V. Blood flow: magnetic resonance imaging. *Radiology* **1985**;154:443–450
28. Axel L. Blood flow effects in magnetic resonance imaging. *AJR* **1984**;143:1157–1166
29. Bradley WG, Waluch V, Ka-Siu L, Fernandez EJ, Spalter C. The appearance of rapidly flowing blood on magnetic resonance images. *AJR* **1984**;143:1167–1174
30. Waluch V, Bradley WG. NMR even echo rephasing in slow laminar flow. *J Comput Assist Tomogr* **1984**;8:594–598
31. Schultz CL, Alfidi RJ, Nelson AD, Kopiwoda SY, Clampitt ME. The effect of motion on two-dimensional fourier transformation magnetic resonance images. *Radiology* **1984**;152:117–121
32. George CR, Jacobs G, MacIntyre WJ, et al. Magnetic resonance signal intensity patterns obtained from continuous and pulsatile flow models. *Radiology* **1984**;151:421–428
33. Singer JR. NMR diffusion and flow measurements and an introduction to spin phase graphing. *J Phys E Sci Instrum* **1978**;11:281–291
34. Jones DW, Child TF. NMR in flowing systems. In: Waugh JS, ed. *Advances in magnetic resonance*, vol 8. New York: Academic, **1976**:123–148
35. Di Chiro G, Schellinger D. Computed tomography of the spinal cord after lumbar intrathecal introduction of metrizamide (computer assisted myelography). *Radiology* **1976**;120:101–104
36. Isherwood I, Fawcitt R, Forbes W. Computed tomography of the spinal canal using metrizimide. *Acta Radiol [Suppl]* (Stockh) **1977**;355:299–305
37. Rubin JB, Enzmann DR. Harmonic modulation of proton MR precessional phase by pulsatile motion: origin of spinal CSF flow phenomena. *AJNR* **1987**;8:307–318
38. Jirout VJ, Fisher J, Nadvornik F. Anatomic and pneumographic studies of the posterior arachnoid space of the normal thoracic spine. *ROFO* **1964**;101:395–399
39. Patel JP, Ramesh NV. *Basic hemodynamics and its role in disease processes.* Baltimore: University Park, **1980**
40. McDonald DA. *Blood flow in arteries*, 2nd ed. Baltimore: Williams & Wilkins, **1974**
41. Rubin JB, Enzmann DR. Optimizing conventional MR spine imaging. *Radiology* **1987** (in press)
42. Rubin JB, Enzmann DR, Wright A. CSF gated spine MRI: theory and clinical implementation. *Radiology* **1987** (in press)